AIAA JOURNAL
Vol. 30, No. 11, November 1992

Comparison of Algebraic Turbulence Models for Afterbody Flows with Jet Exhaust

William B. Compton III*
NASA Langley Research Center, Hampton, Virginia 23681
Khaled S. Abdol-Hamid†
Analytical Services and Materials, Inc., Hampton, Virginia 23666
and
William K. Abeyounis‡
NASA Langley Research Center, Hampton, Virginia 23681

Three-dimensional Navier-Stokes simulations have been done for transonic and low supersonic flow past a nonaxisymmetric nozzle typical of those advocated for advanced fighter airplanes. The jet exhaust is included in the calculations. The investigation compares the performance of the unmodified Baldwin-Lomax turbulence model with its performance when enhanced by the Degani-Schiff and the Goldberg modifications. Solutions are presented for Mach numbers of 0.80, 0.94, and 1.20 at 0-deg angle of attack and a Reynolds number of 20×10^6. The numerical results, which are compared to the wind-tunnel data, show that the three turbulence models predict considerably different shock locations, separated-flow regions, and flowfields.

Nomenclature

A, B, C_1, C_2 = constants in the Goldberg modification for turbulence models
A^+, C_{cp}, k = constants in the Baldwin-Lomax turbulence model
C_p = pressure coefficient, $(p - p_\infty)/q_\infty$
F_{Kleb} = Klebanoff intermittency factor [see Eq. (7)]
$F(n)$ = function in the Baldwin-Lomax turbulence model [see Eq. (6)]
$\hat{F}, \hat{G}, \hat{H}$ = flux vectors in the transformed coordinate ξ, η, ζ directions respectively
$\mathcal{G}$ = Gaussian [see Eq. (8)]
K = Clauser constant
L = reference length, length of model from nose to jet exit (63 in.)
ℓ = mixing length for turbulent viscosity
M_∞ = free-stream Mach number
n = normal distance from the wall
n^+ = law-of-the-wall coordinate, $(n\sqrt{\rho_w \tau_w})/\mu_w$
p = pressure
$\hat{Q}$ = transformed vector of dependent flow variables
q_∞ = freestream dynamic pressure, $\frac{1}{2}\rho_\infty(u_\infty^2 + v_\infty^2 + w_\infty^2)$
R = Reynolds number based on length of model from nose to nozzle exit
t = time
u_s = velocity scale for separated flows [see Eq. (8)]
u, v, w = velocities in the physical coordinate directions x, y, z, respectively
x, y, z = physical (Cartesian) coordinates in the axial, horizontal, and vertical directions respectively, (origin at nose of model)
α = angle of attack, deg
μ = viscosity
ξ, η, ζ = generalized coordinates in transformed coordinate system (approximately the axial, circumferential, and radial directions)
ρ = density
τ_w = local shear stress at wall
ω = vorticity

Subscripts

i = inner
max = maximum
min = minimum
o = outer
s = separated
t = turbulent
w = wall
∞ = freestream conditions

Unless otherwise noted, all variables in this paper are nondimensionalized by appropriate combinations of the free-stream parameters and the reference length L.

Introduction

THE afterbody drag of a typical fighter airplane can be as high as one-half of the total drag of the airplane.[1] Consequently, when integrating the propulsion system and airframe of a fighter, designers spend a great deal of effort in predicting and analyzing the afterbody flow to derive a configuration with the highest possible performance. Although panel methods[2] have been used to predict the afterbody flow, the flow's highly viscous and complex nature requires that Navier-Stokes techniques be used to adequately model the physics.

Swanson,[3] Deiwert and Rothmund,[4] and Vatsa et al.[5] did some of the earlier work in applying the Navier-Stokes equations to the afterbody problem. However, none of these investigations solved the three-dimensional Navier-Stokes equations for the external afterbody flow at transonic speeds or included the jet at transonic speeds. Also, all these computa-

Received April 2, 1991; revision received March 30, 1992; accepted for publication April 10, 1992.

*Aeronautical Engineer, Propulsion Aerodynamics Branch, Applied Aerodynamics Division. Senior Member AIAA.
†Senior Scientist. Member AIAA.
‡Aerospace Engineer, Propulsion Aerodynamics Branch, Applied Aerodynamics Division. Member AIAA.

tions were done only with two-layer algebraic turbulence models such as the Baldwin-Lomax model. The authors of Ref. 6 extended the application of the three-dimensional Navier-Stokes equations to the afterbody problem by solving for transonic flow over a nonaxisymmetric nozzle typical of those being advocated for advanced fighters. The jet exhaust in Ref. 6 was represented by a solid sting. The authors of Ref. 7 further extended the application by solving for supersonic flow over this same configuration with different turbulence models.

The solutions in Refs. 6 and 7 generally agree very well with data for attached flow. However, the results point out several areas for improvement, one of which is predicting massively separated flows. The solutions confirm that, although the unmodified Baldwin-Lomax turbulence model gives very good results for attached flow, It is inadequate when regions of massive separation exist. Also, Ref. 7 shows that, at a Mach number of 1.2, more advanced turbulence models improve the solution for at least some massively separated flows.

The present investigation focuses on this problem. It compares the performance of three algebraic turbulence models, the unmodified Baldwin-Lomax model,[8] and the Baldwin-Lomax model enhanced by the Degani-Schiff[9] and Goldberg[10] and Goldberg and Chakravarthy[11] modifications, in calculating afterbody flow at transonic and low supersonic speeds. The jet exhaust is included in the calculations. The computations were done with the multiple block version of the PAB3D code,[12-14] which solves the three-dimensional thin-layer Reynolds-averaged Navier-Stokes equations and features a numerical algorithm based on upwind differencing. The present investigation was conducted at freestream Mach numbers of 0.80, 0.94, and 1.20, at an angle of attack of 0 deg, and at a Reynolds number of approximately 20×10^6 based on the model length. The calculations are compared with experimental data.

Governing Equations

The Navier-Stokes equations mathematically model the physical laws governing the motion of a compressible fluid with dissipation. In PAB3D, the three-dimensional, time-dependent, Reynolds-averaged Navier-Stokes equations are normalized and written in strong conservation form for a Cartesian coordinate system (x, y, z). Body forces play an insignificant role in the afterbody flow problem and are neglected. Since the dominant dissipative effects for the problem arise mainly from diffusion normal to the afterbody surface, a thin-layer option was chosen that retains only the diffusion terms normal to the body surface. The resulting time-dependent equations for the conservation of mass, linear momentum, and energy can be expressed in terms of a fixed, generalized coordinate system (ξ, η, ζ) as

$$\hat{Q}_t + \hat{F}_\xi + \hat{G}_\eta + (\hat{H}-\hat{H}_v)_\zeta = 0 \tag{1}$$

The relations between the energy, pressure, and enthalpy for an ideal gas complete the system of equations.

Turbulence Models

Turbulent viscosity is modeled by three algebraic formulations. The first, the unmodified Baldwin-Lomax turbulence model[8] is a two-layer model that follows the pattern of Cebeci[15] but avoids the necessity of determining the boundary-layer thickness. The second formulation is the Baldwin-Lomax model with the Degani-Schiff[9] modification for strong vortical flow. The third is the Baldwin-Lomax model with the Goldberg modification.[10,11] With the Goldberg modification, the model can be considered a three-layer turbulence model, where the third layer is used to simulate the separated regions of the flow.

Baldwin-Lomax Model

The Baldwin-Lomax model[8] is an algebraic two-layer turbulence model where the turbulent viscosity is evaluated as follows:

$$\mu_t = (\mu_t)_i \qquad \text{for} \qquad n \le n_{\text{cros}}$$

$$\mu_t = (\mu_t)_o \qquad \text{for} \qquad n > n_{\text{cros}}$$

where n is the normal distance from the wall, and n_{cros} is the smallest value of n at which magnitudes of $(\mu_t)_i$ and $(\mu_t)_o$ are equal.

For the inner layer,

$$(\mu_t)_i = \rho \ell^2 |\omega| \tag{2}$$

where

$$\ell = kn[1 - \exp(-n^+/A^+)]$$

$$n^+ = (\sqrt{\rho_w \tau_w}/\mu_w)n \tag{3}$$

and

$$\omega = \sqrt{(u_y - v_x)^2 + (v_z - w_y)^2 + (w_x - u_z)^2} \tag{4}$$

For the outer layer,

$$(\mu_t)_o = KC_{cp}\rho F_{\text{wake}} F_{\text{Kleb}}(n) \tag{5}$$

where F_{wake} is the smaller of

$$\begin{cases} n_{\max} F_{\max} \\ C_{wk} n_{\max} (u^2 + v^2 + w^2)_{\max}/F_{\max} \end{cases}$$

The term $n_{\max}$ is the value of n corresponding to the maximum value of F, $F_{\max}$, where

$$F(n) = n|\omega|[1 - \exp(-n^+/A^+)] \tag{6}$$

and F_{Kleb} is calculated by

$$F_{\text{Kleb}} = [1 + 5.5(nC_{\text{Kleb}}/n_{\max})^6]^{-1} \tag{7}$$

The values of the constants appearing in Eqs. (2-7) are listed in Ref. 8 as

$$A^+ = 26, \qquad C_{wk} = 0.25$$

$$C_{cp} = 1.6, \qquad k = 0.4$$

$$C_{\text{Kleb}} = 0.3, \qquad K = 0.0168$$

Degani-Schiff Modification

Degani and Schiff[9] modified the Baldwin-Lomax turbulence model to more accurately determine the outer length scale when a strong vortical flow structure, such as a massive separation, exists. For these flows they discovered that, at a given streamwise station, the quantity $F(n)$ [Eq. (6)] has more than one local maximum, or peak. Furthermore, the largest peak is always associated with the radial distance from the body to the edge of the backflow region, and its use can result in an outer eddy viscosity that is as much as two orders of magnitude too high.

Hence, Degani and Schiff recommend using the local maximum in $F(n)$ associated with the underlying backflow. To avoid selecting extraneous fluctuations, they chose the first well-defined peak away from the wall, where a well-defined peak in $F(n)$ is defined as a peak where $F(n)$ drops to $<90\%$ of its local maximum value.

Goldberg Modification

Goldberg[10] and Goldberg and Chakravarthy[11] introduced a modification for boundary-layer turbulence models that is

designed to simulate the separation bubble in the flow. The modification consists of a simple formula for the distribution of the eddy viscosity within the bubble. In the present work their modification is applied to the Baldwin-Lomax model.

For high-Reynolds-number flows, Goldberg and Chakravarthy[11] show that the viscosity in the separation regions can be evaluated as

$$(\mu_t)_s = C_1 u_s n_s \sqrt{\rho_w \rho}[A(n/n_s) + B]\sqrt{\mathcal{G}(n)} \quad \text{for} \quad 0 < n < n_s \tag{8}$$

$$(\mu_t)_v = C_2 u_s n_s \sqrt{\rho_w \rho} \quad \text{for} \quad n_s \le n < n_{cr} \tag{9}$$

where u_s is a velocity scale defined as the square root of the maximum vorticity times the corresponding turbulence viscosity, and $\mathcal{G}$ is the Gaussian given in Ref. 11. The values of the constants A, B, C, and C_2 are given in Ref. 11 as

$$C_1 \approx 0.353, \qquad A = -0.151$$

$$C_2 \approx 0.188, \qquad B = 0.684$$

Beyond the edge of the backflow region, Eq. (9) is used up to n_{cr}, the smallest value of n at which the values of μ_t from Eq. (9) and the Baldwin-Lomax model are equal. Beyond this point, the Baldwin-Lomax model is used. The edge of the backflow region, n_s, is treated as a wall boundary; thus, n in Eqs. (3) and (5-7) is replaced by $n - n_s$.

Procedure

Computational Domain and Grid

Figure 1 illustrates the computational domain, grid topology, and coordinate system. For clarity, the figure depicts every other grid point. Figure 2 illustrates the model and defines the afterbody, or nozzle, which is the region of interest in this investigation.

To minimize computer resources, symmetry is assumed about the vertical plane containing the model axis, and the computational domain is composed of only one-half of a cylinder (see Fig. 1). The domain extends one model length (~ 20 model radii) upstream from the model nose and an equal distance downstream from the jet exit. The far-field boundaries ($\zeta = \zeta_{max}$) are also ~ 20 model radii from the model surface.

The computational grid is body fitted (grid lines coincide with the model surface and other boundaries) to facilitate implementation of the boundary conditions. The mesh (excluding the jet exhaust region) contains 129 planes axially (29 on the afterbody), 65 radially, and 33 circumferentially. The mesh density in the exhaust plume is $29 \times 40 \times 33$ in the corresponding directions.

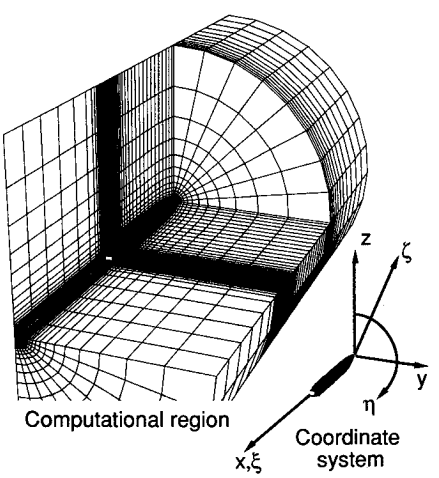

Fig. 1 Three-dimensional computation domain, grid, and coordinate system (every other grid line is depicted for clarity).

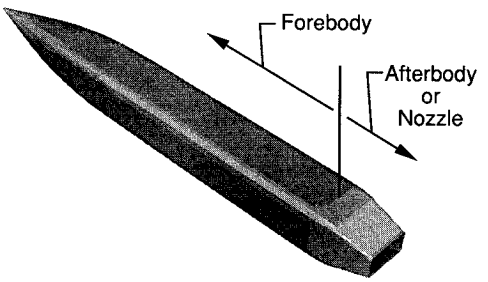

Fig. 2 Model illustrating the afterbody or nozzle.

Numerical Algorithm

The solutions were obtained with the multiple-block version of the PAB3D code,[12-14] which solves the three-dimensional Reynolds-averaged thin-layer Navier-Stokes equations. It employs the finite-volume principle where the spatial derivatives in the equations are evaluated as conservative flux balances across the grid cells. The fluxes at the cell interfaces are determined with upwind-biased flux-difference splitting combined with a gradient limiting procedure to ensure monotonicity across discontinuities such as shock waves. The scheme is spatially third-order accurate.

The time-differencing algorithm used in the computational procedure is an approximately factored alternating-direction-implicit scheme in delta form. The terms in the crossflow directions are approximately factored, whereas the terms in the axial, or main flow, direction are split and added to the two resulting factors.

Boundary Conditions

The boundary conditions at the computational domain's inflow boundary ($\xi = 1$) depended on the freestream Mach number (refer to Fig. 1 for the grid topology). With a subsonic freestream, Riemann invariants for a one-dimensional flow were used to calculate the primative flow variables ρ, u, v, w, and p. With a supersonic freestream, all of the variables were specified.

Since the velocity normal to the far-field boundary ($\zeta = \zeta_{max}$) was always subsonic, Riemann invarients were used exclusively to calculate the primative flow variables at this boundary. Reflection boundary conditions were imposed at the vertical plane of symmetry ($\eta = 1$ and $\eta = \eta_{max}$) and on the domain's centerline ($\zeta = 1$ ahead of and behind the model). At the outflow boundary ($\xi = \xi_{max}$), where the flow is a mixture of the jet exhaust and the freestream, all gradients were set to zero regardless of the freestream conditions.

At the jet exit ($\xi = \text{const}$), which is a supersonic inflow boundary, all flow variables for the jet exhaust were specified. The values of the flow variables at the jet exit were calculated by solving for laminar flow inside the nozzle.[16] Finally, a no-slip and an adiabatic wall boundary condition were imposed on the body surface ($\zeta = 1$).

Experimental Data and Model

The experimental data, which were obtained in the NASA Langley 16-Foot Transonic Tunnel,[17] are part of a broad data base for a nonaxisymmetric nozzle typical of those advocated for advanced fighter airplanes. Parts of the data base have been published in Refs. 6, 7, 16, and 18.

The nozzle has external boattail angles of 17.6 deg on the top and bottom and 6.9 deg on the sides, and has a superelliptic external cross section. The internal geometry is rectangular, with flat sidewalls, a 2.6 deg divergence angle on the top and bottom walls, and an exit aspect ratio of 1.9. The design jet total pressure ratio of the nozzle is 4.25, which gives an exit

Mach number of 1.6. The model configuration, including both the external and internal nozzle geometries, is described in detail in Refs. 6 and 18.

The experimental data were taken with the jet exhaust simulated with high-pressure air at a total temperature nominally equal to 544°R. For comparison, the freestream total temperature varied from approximately 606°R at a freestream Mach number of 0.80 to 625°R at a freestream Mach number of 1.20. The jet total pressure ratio was 4.0, a value close to design. During the experiment, boundary-layer transition from laminar to turbulent flow was fixed at 1 in. from the nose of the model (at an x/L of 0.016) with a 0.1-in.-wide strip of no. 90 grit. The absolute error in the freestream Mach number is no more than ± 0.004 (see Ref. 17.) The accuracies in the afterbody pressure coefficients are ± 0.0116, ± 0.0097, and ± 0.0080 at the freestream Mach numbers of 0.80, 0.94, and 1.20, respectively.

Results

Navier-Stokes solutions were obtained for the nonaxisymmetric afterbody at freestream Mach numbers of 0.80, 0.94, and 1.20 and an angle of attack of 0 deg. The corresponding Reynolds numbers were 19.5, 20.2, and 20.5×10^6, respectively.

Convergence

A brief grid study had previously been done for a baseline body-sting configuration and grid topology. The numerical experiments investigated meshes with densities of $64 \times 32 \times 10$ and $257 \times 129 \times 65$ as well as the present mesh of $129 \times 65 \times 33$ (see Refs. 6 and 7). The results obtained at freestream Mach numbers of 0.8 and 1.2 indicate that the solutions are essentially grid converged for the present mesh.

Numerical convergence for the present investigation is based on the residual and the computed pressures. Figure 3

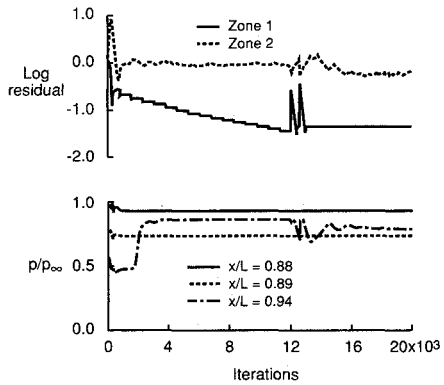

Fig. 3 History of the residual and selected afterbody pressures (Goldberg turbulence model, $M_\infty = 1.20$, pressures on top centerline of afterbody).

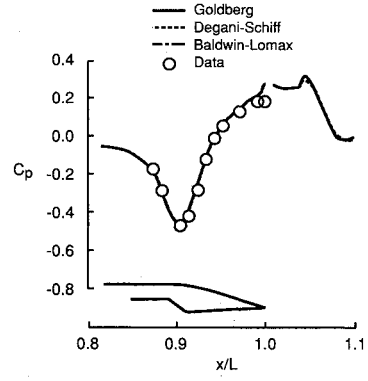

Fig. 4 Afterbody pressure coefficients at $M_\infty = 0.80$ ($\alpha = 0$ deg, $R = 19.5 \times 10^6$, top row).

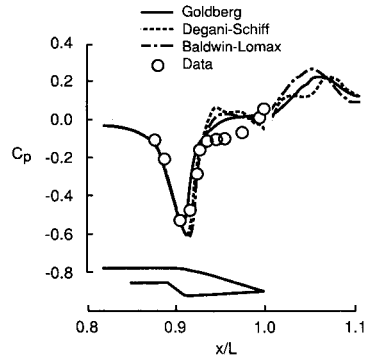

Fig. 5 Afterbody pressure coefficients at $M_\infty = 0.94$ ($\alpha = 0$ deg, $R = 20.2 \times 10^6$, top row).

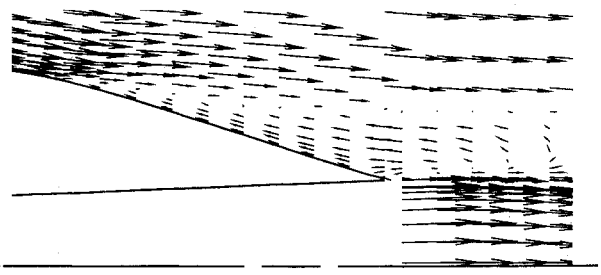

Fig. 6 Velocity vectors in the vertical plane of symmetry ($M_\infty = 0.94$, $\alpha = 0$ deg, $R = 20.2 \times 10^6$, top half of plane, Goldberg turbulence model). Most of the grid points not shown for clarity.

depicts the convergence history of the residuals in zone 1 (ahead of the nozzle exit) and zone 2 (behind the nozzle exit) and of selected afterbody pressures. The results are for a freestream Mach number of 1.20 and the Goldberg turbulence model. The solution was started with uniform flow and a laminar jet plume. The afterbody pressure at an $x/L = 0.94$ initially changes up to 5000 iterations, probably due to its proximity to the afterbody shock, which slowly settles into a steady-state position. The perturbations originating at 12,000 iterations are due to solving the nozzle internal flow between 12,000 and 14,000 time steps and to starting turbulence in the jet plume at 12,000 time steps. The solution is essentially converged after 17,000 iterations.

Solution Strategy

Calculations have previously been done at a freestream Mach number of 1.2 with the turbulent viscosity simultaneously included in the circumferential and radial directions. The pressures predicted along the top centerline of the afterbody were essentially the same as those obtained from thin-layer calculations. Hence, the present study was limited to solving the thin-layer equations in the ζ direction only (which retain only those diffusion terms nominal to the body surface and jet plume) to conserve computer resources.

In the present investigation the jet plume was included in the Navier-Stokes calculations. The turbulent flow downstream of the jet exit was calculated with a modified version[14] of the Jones-Launder two-equation turbulence model.[19] This model was used downstream of the jet exit because of the relative ease in defining the mixing length in the shear layer with a two-equation model.

As stated previously, the boundary layer in the vicinity of the afterbody contained at least 30 grid points normal to the surface. The value of the law-of-the-wall coordinate n^+ for the first grid point off the wall was at most 5, and was generally about 3.

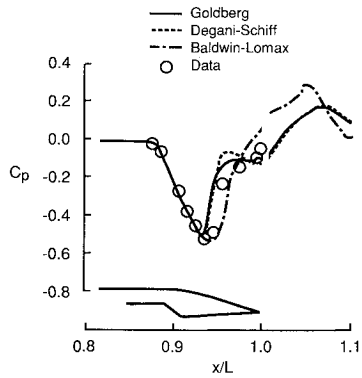

Fig. 7 Afterbody pressure coefficients at $M_\infty = 1.20$ ($\alpha = 0$ deg, $R = 20.5 \times 10^6$, top row).

Freestream Mach Number = 0.80

Figure 4 presents the calculated pressure coefficient distributions along the top centerline of the nozzle at a freestream Mach number of 0.80. The pressure coefficients behind the nozzle exit are located on an imaginary line extending from the lip of the exit and lying parallel to the model axis. The corresponding wind-tunnel pressure data are also included. The pressure data indicate that at this Mach number the flow is essentially attached to the entire afterbody.

Under these conditions all three turbulence models yield virtually the same solution except very near the jet exit where the Goldberg model does slightly better than the other two. The calculations correlate well with the data over most of the nozzle and capture the suction pressure peak exceptionally well as the flow expands around the boattail shoulder. The computed oil flows (not presented) for all three turbulence models show a very small separated region near the nozzle exit. The region is extremely thin and therefore has a negligible effect on the afterbody pressures.

Freestream Mach Number = 0.94

Figures 5 and 6 present the results at the freestream Mach number of 0.94. At this Mach number, the wind-tunnel data indicate obvious shock-induced separation on the top of the nozzle (see the pressure distributions in Fig. 5). Figure 6 presents the computed velocity vectors in the vertical plane containing the model axis. The extent of the reverse flow near the model surface and downstream of the exit indicates that the separation is massive. (Note that not all of the grid points are shown on the plot. Many are left out of the figure so that a clear picture of the vector patterns can be shown.) Although Fig. 6 presents the results for the Goldberg turbulence model, at this Mach number, 0.94, all three turbulence models tested give a similar flow structure.

The calculated pressures agree well with the data up to the location of the shock (refer to Fig. 5). Aft of this point, the turbulence models vary considerably in their predictive capabilities. The unmodified Baldwin-Lomax model predicts the shock induced separation point too far aft, a result typical of eddy-viscosity turbulence models.[20,21] In addition, it produced a recompression after the shock that is too large. The Degani-Schiff modification predicts the shock location better. However, the recompressed pressures it predicts downstream of the shock are no closer to the experimental values than those calculated with the Baldwin-Lomax model.

The Goldberg modification gives a shock that is slightly upstream of the experimental postition. It predicts the pressure level in the separated flow region behind the shock better than the other two models; however, there is still a fairly large discrepancy between the calculated pressures and the data in this region. More advanced turbulence models may yield better results for these types of massively separated flows.[20,21]

At this freestream Mach number, 0.94, the Degani-Schiff modification never yielded a solution that converged to a truly steady state. After approximately 9,000 iterations the pressures in the shock-induced separation zone (aft of $x/L = 0.94$) appeared to oscillate about a constant value, which caused an asymmetry between the flow on the top and bottom of the afterbody. Upstream of the shock, the pressures were steady and the flow was symmetric. Previous calculations with laminar flow downstream of the jet exit exhibited this phenomena for all the turbulence models tested whenever there were strong shocks and massive separation on the afterbody. The result was also noticed in Ref. 16 where the code CFL3D (Ref. 22) was used. Experimental data that would indicate whether or not the flow is actually time dependent are not available.

Freestream Mach Number = 1.20

At the freestream Mach number of 1.20, the experimental data indicate essentially the same features as those at the Mach number of 0.94: an expansion over the initial part of the afterbody followed by shock-induced separation and the associated pressure recovery (see Fig. 7). Again, all three turbulence models yield the same solution up to the point of shock-induced separation.

The differences in the solutions from the shock aft are even greater at this freestream Mach number than they are at the Mach number of 0.94. The unmodified Baldwin-Lomax model predicts the shock location too far downstream as it did previously. In addition, at this Mach number, its pressure distribution shows no clear evidence of a plateau associated with shock-induced separation. The Degani-Schiff and Goldberg models both predict the shock too far upstream. They predict a pressure plateau behind the shock (x/L from 0.94 to 0.99) that is much more pronounced than the data indicate. Again, the Goldberg model predicts the pressure distributions in this region the best.

A more complete understanding of the nature of the afterbody flow and of the difference in the solutions produced by the three turbulence models can be gained by considering Figs. 8-10. The figures illustrate the structure of the flowfield produced by the unmodified Baldwin-Lomax and the Goldberg turbulence models. The Degani-Schiff model gives a structure similar to the one given by the Goldberg model and therefore is not presented.

Figure 8 shows the particle traces, or computed oil flows, on the afterbody at the freestream Mach number of 1.20. The particle traces, which reflect the pressure distributions shown in Fig. 7, show a large separated-flow region on the top of the nozzle and attached flow on its sides. The particle traces depict a significantly different flow structure and a much smaller

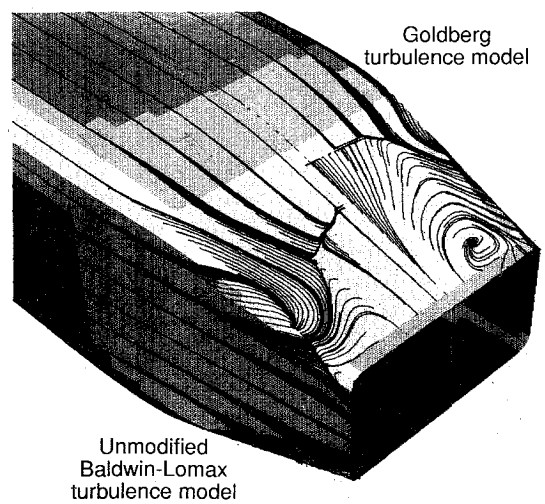

Fig. 8 Afterbody particle traces, i.e., computed oil flows ($M_\infty = 1.20$, $\alpha = 0$ deg, $R = 20.5 \times 10^6$).

separated-flow region for the unmodified Baldwin-Lomax model than for the other two turbulence models.

Figure 9 presents the velocity vectors in the vertical plane of symmetry. The scale is kept the same as the scale in Fig. 6 for $M_\infty = 0.94$ in order to show the relative size of the separated regions at the two Mach numbers. The figure shows that at this Mach number the unmodified Baldwin-Lomax model produces a shock-induced separated region so thin that the reverse flow next to the model surface is not apparent. As a result, the separation has a negligible effect on the effective shape of the afterbody, probably accounting for the lack of a pressure plateau behind the shock (Fig. 7). In contrast, the Degani-Schiff and Goldberg models yield a vastly thicker separated zone (Fig. 9) that effectively modifies the afterbody contour and produces a pressure plateau.

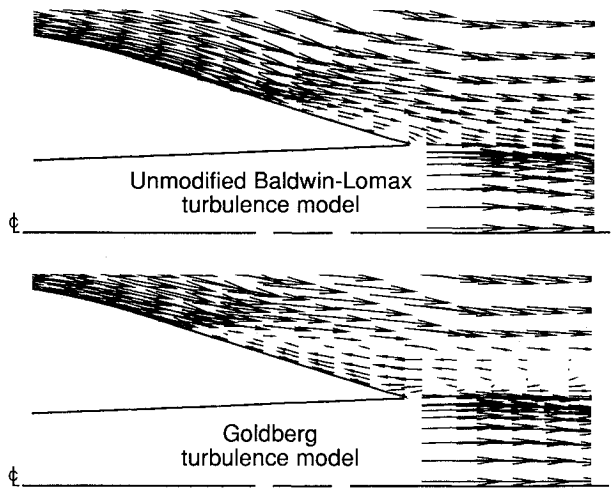

Fig. 9 Velocity vectors in the vertical plane of symmetry ($M_\infty = 1.20$, $\alpha = 0$ deg, $R = 20.5 \times 10^6$, top half of plane). Most of the grid points not shown for clarity.

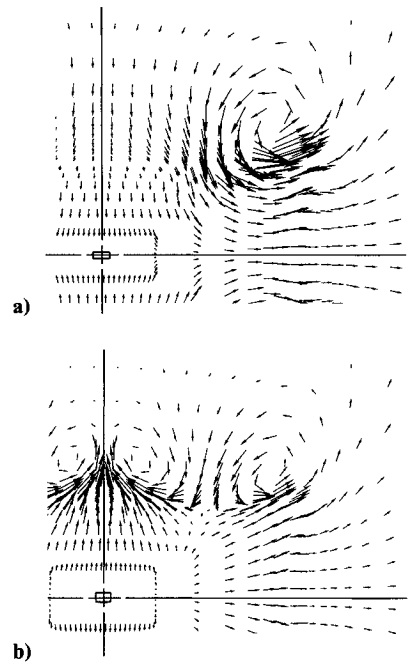

Fig. 10 Crossflow velocity vectors downstream of the nozzle exit ($M_\infty = 1.20$, $\alpha = 0$ deg, $R = 20.5 \times 10^6$, looking upstream, upper right quadrant). Most of the grid points not shown for clarity: a) unmodified Baldwin-Lomax turbulence model, b) Goldberg turbulence model).

Figure 10 presents the corresponding crossflow velocity vectors downstream of the nozzle exit. (Only the upper right-hand quadrants are presented.) The crossflow vectors, which are at an $x/L = 1.09$ show that vortices shed from the afterbody. Similar vortices were noticed in Ref. 6 and are seen experimentally in Ref. 18. In the unmodified Baldwin-Lomax solution, vortices trail from the four corners of the nozzle (see Fig. 10a). An examination of the particle traces downstream of the nozzle exit shows that the flow coming off the top and bottom surface of the nozzle divides at the vertical plane through the nozzle axis. It then sweeps outboard toward the corners of the nozzle, creating the vortex structure shown.

In the Degani-Schiff and Godlberg solutions, the flow divides approximately halfway between the center plane and the side of the nozzle. The inboard half sweeps inward toward the center plane and the outboard half toward the sides, producing another pair of vortices near the center (see Fig. 10b). The experimental total-pressure measurements[18] clearly indicate a vortex-like structure at the corners (Fig. 10a). Although there is an additional loss of total pressure near the centerplane, the data are inconclusive concerning the existence of the center pair of vortices. At the freestream Mach numbers of 0.80 and 0.94, the solutions also show vortices behind the nozzle; however, their structure is not always identical to their structure at the Mach number of 1.20.

Future Research and Needs

The difference in the flows produced by the three turbulence models illustrates the need to investigate more advanced turbulence models for the afterbody problem. The previous results also demonstrate the need for comprehensive experiments with detailed measurements to validate Navier-Stokes codes and turbulence models.

In general, off-body and skin-friction data are the types that are most lacking in the afterbody propulsion area. In the present case, detailed velocity and pressure measurements are needed in the near flowfield to map shocks and separated regions. Measurements of both mean and fluctuating velocity components are needed in the boundary layer to help evaluate existing turbulence models and guide the formulation of new ones. In addition, skin-friction, hot-film, and both on- and off-body flow visualization data are needed to further evaluate the solutions.

Concluding Remarks

Three-dimensional Navier-Stokes simulations have been performed for the transonic flow past a nonaxisymmetric nozzle typical of those advocated for advanced fighter airplanes. The jet exhaust was included in the calculations. The investigation compared the performance of three turbulence models: the unmodified Baldwin-Lomax turbulence model, and the Baldwin-Lomax model when enhanced by the Degani-Schiff and the Goldberg modifications. Solutions were presented for Mach numbers of 0.80, 0.94, and 1.20 at 0-deg angle of attack and a Reynolds number of 20×10^6 based on the model length. The results were compared to wind-tunnel data.

At a freestream Mach number of 0.80, where the experimental pressure distributions indicate no apparent separation on the afterbody, all three turbulence models yielded essentially identical solutions. The calculations correlated well with the wind-tunnel data over most of the nozzle and captured the suction pressure peak exceptionally well as the flow expands around the boattail shoulder.

At freestream Mach numbers of 0.94 and 1.20, a shock and massive separation existed on the afterbody. Under these flow conditions, the pressure distributions calculated with all three turbulence models agreed well with the data up to the point of shock-induced separation. Aft of this point, the three models varied considerably in their predictive powers. The unmodified Baldwin-Lomax model consistently predicted the location of the afterbody shocks downstream of their experimental

position, whereas the Goldberg modification predicted the shocks an equal distance upstream of experiment. The Degani-Schiff modification varied from giving an intermediate shock position that agreed closely with data at a Mach number of 0.94 to an upstream position at the Mach number of 1.20. The Goldberg model yielded the most accurate pressure level in the separated region after the shock, although all of the models missed the level by a substantial amount.

At the freestream Mach number of 1.20, the Goldberg and Degani-Schiff modifications gave a considerably different flow structure than the unmodified Baldwin-Lomax model gave. At the freestream Mach numbers of 0.80 and 0.94, all the models predicted a flow structure that was similar to each other.

Considering the variation in the computed flow-fields produced by the three turbulence models, the suitability of other classes of turbulence models for calculating afterbody flow needs to be investigated. These results also point out the need for detailed experiments to validate Navier-Stokes codes and turbulence models.

References

[1]Capone, F. J., "The Nonaxisymmetric Nozzle—It is for Real," AIAA Paper 79-1810, Aug. 1979.

[2]Carlson, J. R., "Evaluation and Application of VSAERO to a Nonaxisymmetric Afterbody with Thrust Vectoring," Society of Automotive Engineers, TP 871775, Oct. 1987.

[3]Swanson, R. C., Jr., "Numerical Solutions of the Navier-Stokes Equations for Transonic Afterbody Flows," NASA TP-1784, Dec. 1980.

[4]Deiwert, G. S., and Rothmund, H., "Three-Dimensional Flow Over a Conical Afterbody Containing a Centered Propulsive Jet: A Numerical Simulation," AIAA Paper 83-1709, July 1983.

[5]Vatsa, V. N., Thomas, J. L., and Wedan, B. W., "Navier-Stokes Computations of Prolate Spheroids at Angle of Attack," AIAA Paper 87-2627, Aug. 1987.

[6]Compton, W. B., III, Thomas, J. L., Abeyounis, W. K., and Mason, M. L., "Transonic Navier-Stokes Solutions of Three-Dimensional Afterbody Flows," NASA TM-4111, July 1989.

[7]Abdol-Hamid, K. S., and Compton, W. B., III, "Supersonic Navier-Stokes Simulation of Turbulent Afterbody Flows," AIAA Paper 89-2194, 1989.

[8]Baldwin, B. S., and Lomax, H., "Thin Layer Approximation and Algebraic Model for Separated Turbulent Flows," AIAA Paper 78-257, Jan. 1978.

[9]Degani, D., and Schiff, L. B., "Computation of Supersonic Viscous Flows Around Pointed Bodies at Large Incidence," AIAA Paper 83-0034, Jan. 1983.

[10]Goldberg, U. C., "Separated Flow Treatment with a New Turbulence Model," *AIAA Journal,* Vol. 24, No. 10, 1986, pp. 1711–1713.

[11]Goldberg, U. C., and Chakravarthy, S., "Separated Flow Predictions Using a Hybrid *K-L*/Backflow Model," *AIAA Journal,* Vol. 28, No. 6, 1990, pp. 1005–1009.

[12]Abdol-Hamid, K. S., "A Multiblock/Multizone Code (PAB 3D-v2) for the Three-Dimensional Navier-Stokes Equations: Preliminary Applications," NASA-CR 182032, Sept. 1990.

[13]Abdol-Hamid, K. S., "Development of Three-Dimensional Code for the Analysis of Jet Mixing Problem—Part I: Laminar Solution," NASA CR-4200, Dec. 1989.

[14]Abdol-Hamid, K. S., Uenishi, K., and Turner, W. M., "Three-Dimensional Upwinding Navier-Stokes Code With k-ϵ Model for Supersonic Flows," AIAA Paper 91-1669, June 1991.

[15]Cebeci, T., "Calculation of Compressible Turbulent Boundary Layers with Heat and Mass Transfer," AIAA 70-0741, June 1970.

[16]Compton, William B., III, and Abdol-Hamid, K. S., "Navier-Stokes Simulation of Nozzle-Afterbody Flows with Jets at Off-Design Conditions," AIAA Paper 91-3207, Sept. 1991.

[17]Corson, B. W., Jr., Runckel, J. F., and Igoe, W. B., "Calibration of the Langley 16-Foot Transonic Tunnel with Test Section Air Removal," NASA TR-R-423, Aug. 1974.

[18]Putnam, L. E., and Mercer, C. E., "Pitot-Pressure Measurements in Flow Fields Behind a Rectangular Nozzle with Exhaust Jet for Free-Stream Mach Numbers of 0.00, 0.60, and 1.20," NASA TM-88990, Nov. 1986.

[19]Jones, W. P., and Launder, B. E., "The Calculation of Low-Reynolds-Number Phenomena with a Two-Equation Model of Turbulence," *International Journal of Heat and Mass Transfer,* Vol. 16, 1973, pp. 1119–1130.

[20]Marvin, J. G., "Turbulence Modeling for Computational Aerodynamics., *AIAA Journal,* Vol. 21, No. 7, July 1983, pp. 941–955.

[21]Lakshminarayana, B., "Turbulence Modeling for Complex Flows," AIAA Paper 85-1652, July 1985.

[22]Thomas, J. L., and Newsome, R. W., "Navier-Stokes Computations of Lee-Side Flows over Delta Wings," AIAA Paper 86-1049, May 1986.